

Conjugate Function Method for Numerical Conformal Mappings

Harri Hakula, Tri Quach, and Antti Rasila

Abstract. We present a method for numerical computation of conformal mappings from simply or doubly connected domains onto so-called canonical domains, which in our case are rectangles or annuli. The method is based on conjugate harmonic functions and properties of quadrilaterals. Several numerical examples are given.

Keywords. numerical conformal mappings, conformal modulus, quadrilaterals, canonical domains.

2010 MSC Primary 30C30; Secondary 65E05, 31A15, 30C85.

1. Introduction

Conformal mappings, besides their theoretical significance in complex analysis, are also important in certain applications, such as electrostatics and aerodynamics [23]. In this paper we study numerical computation of conformal mappings f of a domain $\Omega \subset \mathbb{C}$ into \mathbb{C} . We assume that the domain is bounded and that there are either one or two simple (and non-intersecting) boundary curves, i.e., the domain Ω is either simply or doubly connected. It is usually convenient to map the domains conformally onto canonical domains, which are in our case a rectangle $R_h = \{z \in \mathbb{C} : 0 < \operatorname{Re} z < 1, 0 < \operatorname{Im} z < h\}$ or an annulus $A_r = \{z \in \mathbb{C} : e^{-r} < |z| < 1\}$. While the existence of such conformal mappings is expected because of Riemann's mapping theorem, it is usually not possible to obtain a formula or other representation for the mapping analytically.

Several different algorithms for numerical computation of conformal mappings have been described in literature. One popular method involves the Schwarz-Christoffel formula, which can also be generalized for doubly connected domains. A widely used MATLAB implementation of this method is due to Driscoll [8] and FORTRAN version due to Hu [13]. For theoretical background concerning these methods see [9, 10, 25]. In addition, there are several approaches which do not involve the Schwarz-Christoffel formula, e.g., the Zipper algorithm of

Marshall [19, 20]. For an overview of numerical conformal mappings and moduli of quadrilaterals, see [21]. Historical remarks and outline of development of numerical methods in conformal mappings is given in [9, 17, 22].

In this paper, we present a new method which is based on the harmonic conjugate function and properties of quadrilaterals, which together form the foundation of our numerical algorithm. The algorithm is based on solving numerically the Laplace equation subject to Dirichlet-Neumann mixed-type boundary conditions. The outline of the paper is as follows: First the preliminary concepts are introduced and then the new algorithm is described in detail. Before the numerical examples, the computational complexity and some details of our implementation are discussed. The numerical examples are divided into three sections: validation against the Schwarz-Christoffel toolbox, simply connected domains, and finally ring domains.

2. Foundations of the Conjugate Function Method

In this section we introduce the required concepts from function theory and present a proof of the theorem laying the foundation for the numerical algorithm.

Definition 2.1. (Modulus of a Quadrilateral)

A Jordan domain Ω in \mathbb{C} with marked (positively ordered) points $z_1, z_2, z_3, z_4 \in \partial\Omega$ is called a *quadrilateral*, and denoted by $Q := (\Omega; z_1, z_2, z_3, z_4)$. Then there is a canonical conformal map of the quadrilateral Q onto a rectangle $R_h = (\Omega'; 1+ih, ih, 0, 1)$, with the vertices corresponding, where the quantity h defines the *modulus of a quadrilateral* Q . We write

$$M(Q) = h.$$

Note that the modulus h is unique.

Definition 2.2. (Reciprocal Identity)

It is clear by the geometry [18, p. 15] or [21, pp. 53-54] that the following reciprocal identity holds:

$$(1) \quad M(Q) M(\tilde{Q}) = 1,$$

where $\tilde{Q} = (\Omega; z_2, z_3, z_4, z_1)$ is called the *conjugate quadrilateral* of Q .

For basic properties of modulus of quadrilaterals, we refer to [18] and [21, Chapter 2].

Remark. The identity (1) leads to a method for estimating the numerical accuracy of the modulus. For discussion and several numerical examples see [11].

2.1. Dirichlet-Neumann Problem. It is well known that one can express the modulus of a quadrilateral Q in terms of the solution of the Dirichlet-Neumann mixed boundary value problem [12, p. 431].

Let Ω be a domain in the complex plane whose boundary $\partial\Omega$ consists of a finite number of regular Jordan curves, so that at every point, except possibly at finitely many points of the boundary, a normal is defined. Let $\partial\Omega = A \cup B$ where A, B both are unions of regular Jordan arcs such that $A \cap B$ is finite. Let ψ_A, ψ_B be real-valued continuous functions defined on A, B , respectively. Find a function u satisfying the following conditions:

1. u is continuous and differentiable in $\bar{\Omega}$.
2. $u(t) = \psi_A(t)$, for all $t \in A$.
3. If $\partial/\partial n$ denotes differentiation in the direction of the exterior normal, then

$$\frac{\partial}{\partial n}u(t) = \psi_B(t), \quad \text{for all } t \in B.$$

The problem associated with the conjugate quadrilateral \tilde{Q} is called the *conjugate Dirichlet-Neumann problem*.

Let $\gamma_j, j = 1, 2, 3, 4$ be the arcs of $\partial\Omega$ between $(z_1, z_2), (z_2, z_3), (z_3, z_4), (z_4, z_1)$, respectively. Suppose that u is the (unique) harmonic solution of the Dirichlet-Neumann problem with mixed boundary values of u equal to 0 on γ_2 , equal to 1 on γ_4 and with $\partial u/\partial n = 0$ on γ_1, γ_3 . Then by [1, Theorem 4.5] or [21, Theorem 2.3.3]:

$$(2) \quad M(Q) = \iint_{\Omega} |\nabla u|^2 dx dy.$$

Suppose that Q is a quadrilateral, and u is the harmonic solution of the Dirichlet-Neumann problem and let v be a conjugate harmonic function of u such that $v(\operatorname{Re} z_3, \operatorname{Im} z_3) = 0$. Then $f = u + iv$ is an analytic function, and it maps Ω onto a rectangle R_h such that the image of the points z_1, z_2, z_3, z_4 are $1 + ih, ih, 0, 1$, respectively. Furthermore by Carathéodory's theorem [14, Theorem 5.1.1], f has a continuous boundary extension which maps the boundary curves $\gamma_1, \gamma_2, \gamma_3, \gamma_4$ onto the line segments $\gamma'_1, \gamma'_2, \gamma'_3, \gamma'_4$, see Figure 1.

Lemma 2.3. *Let Q be a quadrilateral with modulus h , and let u be the harmonic solution of the Dirichlet-Neumann problem. Suppose that v is the harmonic conjugate function of u , with $v(\operatorname{Re} z_3, \operatorname{Im} z_3) = 0$. If \tilde{u} is the harmonic solution of the Dirichlet-Neumann problem associated with the conjugate quadrilateral \tilde{Q} , then $v = h^2 \tilde{u}$.*

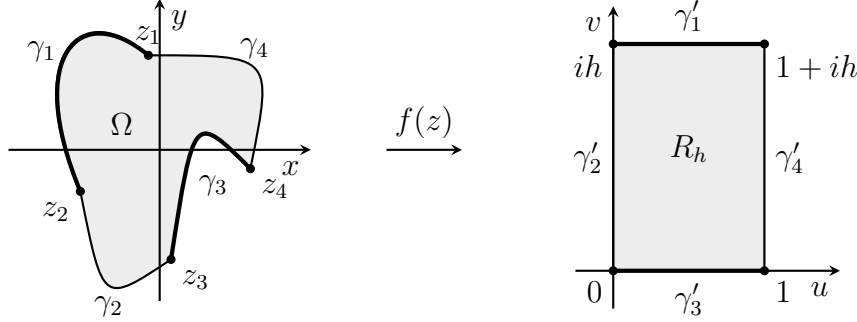


FIGURE 1. Dirichlet-Neumann boundary value problem. Dirichlet and Neumann boundary conditions are mark with thin and thick lines, respectively.

Proof. It is clear that v, \tilde{u} are harmonic. Thus $\tilde{v} = h^2 \tilde{u}$ is harmonic, and v and \tilde{v} have the same values on γ_1, γ_3 . Let $n = (n_1, n_2)$ be the exterior normal of the boundary. Then on γ_2, γ_4 we have

$$\frac{\partial v}{\partial n} = \langle \nabla v, n \rangle = v_x n_1 + v_y n_2 = u_y n_1 - u_x n_2 = 0,$$

because u is constant on γ_2, γ_4 , it follows $u_x = u_y = 0$. Thus v and \tilde{v} also have same values on γ_2, γ_4 . Then by the uniqueness theorem for harmonic functions [2, p. 166] we have $v = \tilde{v}$. \square

Suppose that $f = u + iv$, where u and v are as in Lemma 2.3. Then it is easy to see that the image of equipotential curves of the functions u and v are parallel to the imaginary and the real axis, respectively.

Finally, we note that the function f constructed this way is univalent. To see this, suppose that f is not univalent. Then there exists points $z_1, z_2 \in \Omega$ and $z_1 \neq z_2$ such that $f(z_1) = f(z_2)$. Thus $\operatorname{Re} f(z_1) = \operatorname{Re} f(z_2)$, so z_1 and z_2 are on the same equipotential curve C of u . Similarly for imaginary part, z_1 and z_2 are on the same equipotential curve \tilde{C} of v . Then by the above fact of equipotential curves, it follows that $z_1 = z_2$, which is a contradiction.

2.2. Ring Domains. Let E and F be two disjoint and connected compact sets in the extended complex plane $\mathbb{C}_\infty = \mathbb{C} \cup \{\infty\}$. Then one of the sets E, F is bounded and without loss of generality we may assume that it is E . Then a set $R = \mathbb{C}_\infty \setminus (E \cup F)$ is connected and is called a *ring domain*. The *capacity* of R is defined by

$$\operatorname{cap} R = \inf_u \iint_R |\nabla u|^2 dx dy,$$

where the infimum is taken over all non-negative, piecewise differentiable functions u with compact support in $R \cup E$ such that $u = 1$ on E . Suppose that a function u is defined on R with 1 on E and 0 on F . Then if u is harmonic, it is unique and it minimizes the above integral. The conformal modulus of a ring domain R is defined by $M(R) = 2\pi/\text{cap}R$. The ring domain R can be mapped conformally onto the annulus A_r , where $r = M(R)$. In [3] numerical computation of modulus of several ring domains are studied.

3. Conjugate Function Method

Our aim is to construct a conformal mapping from a quadrilateral $Q = (\Omega; z_1, z_2, z_3, z_4)$ onto a rectangle R_h , where h is the modulus of the quadrilateral Q . Here the points z_j will be mapped onto the corners of the rectangle R_h . If the boundary correspondence is not required, then the points z_1, z_2, z_3, z_4 can be chosen arbitrarily. In the standard algorithm the required steps are the following:

Algorithm 3.1. (*Conformal Mapping*)

1. Find a harmonic solution for a Dirichlet-Neumann problem associated with a quadrilateral.
2. Solve the Cauchy-Riemann differential equations in order to obtain an analytic function that maps our domain of interest onto a rectangle.

The Dirichlet-Neumann problem can be solved by using any suitable numerical method. This method requires solving the Cauchy-Riemann equations. This can be done numerically, see e.g. [4], but it is not necessary, instead we solve v directly from the conjugate problem, which is usually computationally much more efficient, because the mesh and the discretized system used in solving the potential function u can be used for solving v as well.

This new algorithm is as follows:

Algorithm 3.2. (*Conjugate Function Method*)

1. Solve the Dirichlet-Neumann problem to obtain u_1 and compute the modulus h .
2. Solve the Dirichlet-Neumann problem associated with \tilde{Q} to obtain u_2 .
3. Then $f = u_1 + iu_2$ is the conformal mapping from Q onto R_h such that the vertices (z_1, z_2, z_3, z_4) are mapped onto the corners $(1 + ih, ih, 0, 1)$.

In case of ring domains, the construction of the conformal mapping is slightly different. The necessary steps are described below and in Figure 2.

Algorithm 3.3. (*Conjugate Function Method for Ring Domains*)

1. *Solve the Dirichlet problem to obtain the potential function u and the modulus $M(R)$.*
2. *Cut the ring domain through the steepest descent curve which is given by the gradient of the potential function u and obtain a quadrilateral where Neumann condition is on the steepest descent curve and Dirichlet boundaries remains as before.*
3. *Use the Algorithm 3.2.*

Note, that the choice of the steepest descent curve is not unique due to the implicit orthogonality condition.

4. Implementation Aspects

The hp -FEM implementation we are using is described in detail in [11]. For elliptic problems, the superior accuracy of the higher order methods with relatively small number of unknowns has to be balanced against the much higher integration cost and the cost of evaluating the solution at any given point in the domain.

In the context of solution of the conjugate pair problems, it is obvious that we only have to integrate only once. Moreover, the factorization of the resulting discretized systems can be, for the most part, used in both problems without any extra work.

However, the computation of the contour lines necessarily involves a large number of evaluations of the solution, that also become more expensive as the order of the method increases.

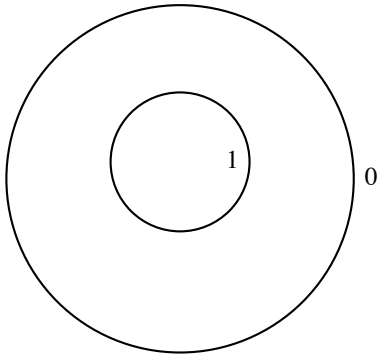
4.1. hp -FEM. In the h -version or standard finite element method, the unknowns or degrees of freedom are associated with values at specified locations of the discretization of the computational domain, that is, the nodes of the mesh. In the p -method, the unknowns are coefficients of some polynomials that are associated with topological entities of the elements, nodes, sides, and interior. Thus, in addition to increasing accuracy through refining the mesh, we have an additional refinement parameter, the polynomial degree p .

Let us next define a p -type quadrilateral element. The construction of triangles is similar and can be found from the references given above.

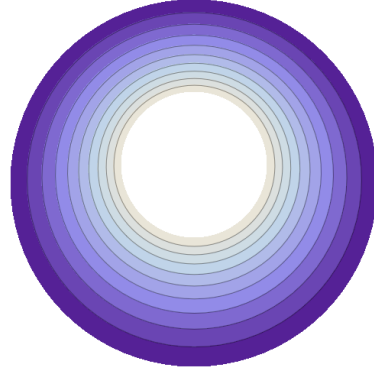
Many different selections of shape functions are possible. We use the so-called hierarchic integrated Legendre shape functions.

Legendre polynomials of degree n can be defined using a recursion formula

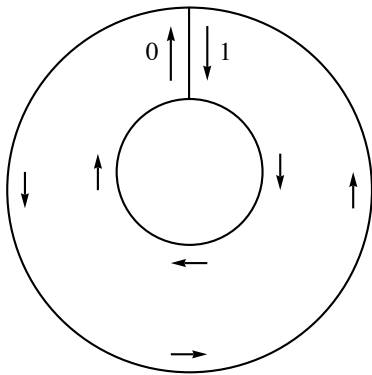
$$(n+1)P_{n+1}(x) - (2n+1)xP_n(x) + nP_{n-1}(x) = 0,$$



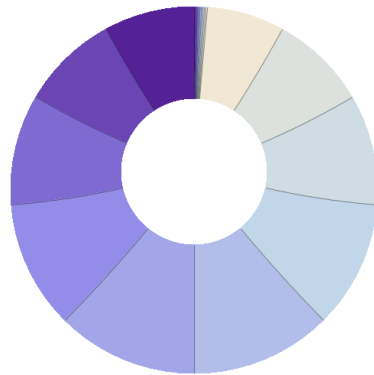
(A) Ring domain with Dirichlet data 0, and 1, on the outer and inner boundaries, respectively..



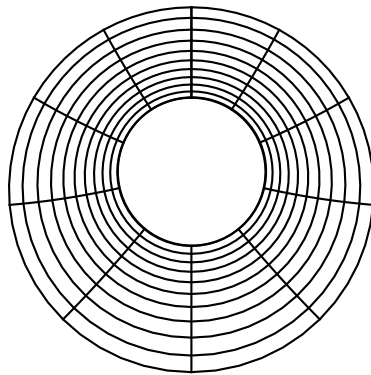
(B) Ring domain: Solution of the Dirichlet problem with contour lines.



(C) Cut domain with new Dirichlet data along the both sides of the cut.



(D) Cut domain: Solution of the conjugate problem with contour lines.



(E) Mapped annulus.

FIGURE 2. Conjugate Function Method for Ring Domains.

where $P_0(x) = 1$ and $P_1(x) = x$.

The derivatives can similarly be computed using a recursion

$$(1 - x^2)P'_n(x) = -nP_n(x) + nP_{n-1}(x).$$

For our purposes the central polynomials are the integrated Legendre polynomials for $x \in [-1, 1]$,

$$\phi_n(\xi) = \sqrt{\frac{2n-1}{2}} \int_{-1}^{\xi} P_{n-1}(t) dt, \quad n = 2, 3, \dots$$

which can be rewritten as linear combinations of Legendre polynomials

$$\phi_n(\xi) = \frac{1}{\sqrt{2(2n-1)}} (P_n(\xi) - P_{n-2}(\xi)), \quad n = 2, 3, \dots$$

The normalizing coefficients are chosen so that

$$\int_{-1}^1 \frac{d\phi_i(\xi)}{d\xi} \frac{d\phi_j(\xi)}{d\xi} d\xi = \delta_{ij}, \quad i, j \geq 2.$$

We can now define the shape functions for a quadrilateral reference element over the domain $[-1, 1] \times [-1, 1]$. The shape functions are divided into three categories: nodal shape functions, side modes, and internal modes.

There are four nodal shape functions.

$$\begin{aligned} N_1(\xi, \eta) &= \frac{1}{4}(1 - \xi)(1 - \eta), & N_2(\xi, \eta) &= \frac{1}{4}(1 + \xi)(1 - \eta), \\ N_3(\xi, \eta) &= \frac{1}{4}(1 + \xi)(1 + \eta), & N_4(\xi, \eta) &= \frac{1}{4}(1 - \xi)(1 + \eta), \end{aligned}$$

which taken alone define the standard four-node quadrilateral finite element. There are $4(p-1)$ side modes associated with the sides of a quadrilateral ($p \geq 2$), with $i = 2, \dots, p$,

$$\begin{aligned} N_i^{(1)}(\xi, \eta) &= \frac{1}{2}(1 - \eta)\phi_i(\xi), & N_i^{(2)}(\xi, \eta) &= \frac{1}{2}(1 + \xi)\phi_i(\eta), \\ N_i^{(3)}(\xi, \eta) &= \frac{1}{2}(1 + \eta)\phi_i(\eta), & N_i^{(4)}(\xi, \eta) &= \frac{1}{2}(1 - \xi)\phi_i(\xi). \end{aligned}$$

For the internal modes we choose the $(p-1)(p-1)$ shapes

$$N_{i,j}^0(\xi, \eta) = \phi_i(\xi)\phi_j(\eta), \quad i = 2, \dots, p, \quad j = 2, \dots, p.$$

The internal shape functions are often referred to as bubble-functions.

The Legendre polynomials have the property $P_n(-x) = (-1)^n P_n(x)$. In 2D all internal edges of the mesh are shared by two different elements. We must ensure that each edge has the same global parameterization in both elements. This additional book-keeping is not necessary in the standard h -FEM.

4.2. Solution of Linear Systems. Let us divide the degrees of freedom of a discretized quadrilateral into five sets, internal and boundary degrees of freedom. The sets are denoted B, D_0, D_1, N^0 , and N^1 , for internal, Dirichlet $u = 0$, Dirichlet $u = 1$, Neumann with Dirichlet $u = 0$ in the conjugate problem, and Neumann with Dirichlet $u = 1$ in the conjugate problem, degrees of freedom, respectively.

The discretized system is

$$A = \begin{pmatrix} A_{BB} & A_{BN^1} & A_{BN^0} & A_{BD_1} & A_{BD_0} \\ A_{N^1B} & A_{N^1N^1} & A_{N^1N^0} & A_{N^1D_1} & A_{N^1D_0} \\ A_{N^0B} & A_{N^0N^1} & A_{N^0N^0} & A_{N^0D_1} & A_{N^0D_0} \\ A_{D_1B} & A_{D_1N^1} & A_{D_1N^0} & A_{D_1D_1} & A_{D_1D_0} \\ A_{D_0B} & A_{D_0N^1} & A_{D_0N^0} & A_{D_0D_1} & A_{D_0D_0} \end{pmatrix}.$$

Taking the Dirichlet boundary conditions into account, we arrive at the following system of equations, using $x_{D_1} = \mathbf{1}$,

$$\begin{pmatrix} A_{BB} & A_{BN^1} & A_{BN^0} \\ A_{N^1B} & A_{N^1N^1} & A_{N^1N^0} \\ A_{N^0B} & A_{N^0N^1} & A_{N^0N^0} \end{pmatrix} \begin{pmatrix} x_B \\ x_{N^1} \\ x_{N^0} \end{pmatrix} = - \begin{pmatrix} A_{BD_1} \mathbf{1} \\ A_{N^1D_1} \mathbf{1} \\ A_{N^0D_1} \mathbf{1} \end{pmatrix}.$$

For the conjugate problem, simply change the roles of $D_1 \leftrightarrow N^1$ and $D_0 \leftrightarrow N^0$. Note that A_{BB} is present in both systems and thus *has to be factored only once*.

4.3. Evaluation of Contour Lines. Let us denote the solutions u and v , respectively. In computing the contour lines, the solutions and their gradients have to be evaluated at many points (x, y) . Evaluation of the solution in hp -FEM is more complicated than in the standard FEM. In a reference-element-based system such as ours, in order to evaluate the solution at point (x, y) one must first find the enclosing element and then the local coordinates of the point on that element. Then every shape function has to be evaluated at the local coordinates of the point. This is outlined in detail in Algorithm 4.1. Similarly evaluation of the gradient of the solution requires two polynomial evaluations per one geometric search.

Algorithm 4.1. (*Evaluation of $u(x, y)$*)

1. Find the enclosing element of (x, y) .
2. Find the local coordinates (ξ, η) on the element.
3. Evaluate the shape functions $\phi_i(\xi, \eta)$.
4. Compute the linear combination of the shape functions $\sum_i c_i \phi_i(\xi, \eta)$, where c_i are the coefficients from the solution vector.

Finding the images of the canonical domains is equivalent to finding the corresponding contour lines of u and v . Since both solutions have been computed on the same mesh, evaluating the solutions and their gradients at the same point is straightforward. In Algorithm 4.2 the two-level line search is described in detail.

Algorithm 4.2. (*Tracing of Contour Lines: $u(x, y) = c = \text{const.}$*)

1. Find the solutions $u(x, y)$ and $v(x, y)$.
2. Set the step size σ and the tolerance ϵ .
3. Choose the potential c .
4. Search along the Neumann boundary for the point (x, y) such that $u(x, y) = c$.
5. Take a step of length σ along the contour line of $u(x, y)$ in the direction of $\nabla v(x, y)$ to a new point (\hat{x}, \hat{y}) .
6. Correct the point (\hat{x}, \hat{y}) by searching in the orthogonal direction, i.e., $\nabla u(\hat{x}, \hat{y})$, until $|u(\hat{x}, \hat{y}) - c| < \epsilon$ is achieved.
7. Set $(x, y) = (\hat{x}, \hat{y})$ and repeat until the opposite Neumann boundary has been reached.

Estimating the computational complexity is complicated, since in the end, the chosen resolution of the image is the dominant factor. In Table 1 the effect of the polynomial degree on the overall execution time is described. As a test case, two by two grid of Figure 2, has been computed using $\sigma = 0.1$, and $\epsilon = \sigma^3$, for $p = 4, 5, 6, 7, 8$. In this particular case we found that doubling of accuracy leads to doubling of time spent in computing the lines. We must emphasize that no attempts to simplify the computations using advanced data structures or techniques have been made and this remains an open and active research topic for application such as mesh generation.

TABLE 1. Effect of p on contour lines computations. Times are normalized so that for $p=4$, time = 1. The reciprocal error refers to the cut domain. In every case 592 iterations of the contour plotting algorithm have been computed.

p	4	5	6	7	8
Time	1	1.21	1.48	1.78	2.16
Reciprocal error	$1.1 \cdot 10^{-5}$	$5.7 \cdot 10^{-7}$	$3.1 \cdot 10^{-8}$	$1.7 \cdot 10^{-9}$	$9.1 \cdot 10^{-11}$

5. Numerical Experiments

Our numerical experiments are divided into three different categories: first we validate the algorithm against the results obtained using the Schwarz-Christoffel

toolbox, then study several examples of using our method to construct a conformal mapping from simply or doubly connected domains onto canonical domains, see Figure 3, with the main results summarized in Tables 2 and 3, respectively.

TABLE 2. Summary of the tests on simply connected domains. Accuracy is given as $\lfloor \log_{10}(1 - M(Q)M(\tilde{Q})) \rfloor$. For the first cases the moduli are known due to symmetry.

Example	ID	$M(Q) / M(\tilde{Q})$	Accuracy	Figure
Unit Disk	5.1	1 / 1	-14	6
Flower	5.2	1 / 1	-11	7
Circular quadrilateral	5.3	0.63058735108478 / 1.585823119159254	-14	8
Asteroidal cusp	5.4	0.68435408764536 / 1.4612318657235575	-10	9

TABLE 3. Summary of the tests on ring domains. Accuracy is given as $\lfloor \log_{10}(1 - M(Q)M(\tilde{Q})) \rfloor$, where the quadrilaterals are those of the cut domain.

Example	ID	$M(R)$	Accuracy	Figure
Disk in regular pentagon	5.5	See Table 5.		10
Cross in square	5.6	0.2862861647287473	-10	11
Circle in square	5.7	0.9920378629010557	-14	12
Flower in square	5.8	0.6669554623348065	-9	13
Circle in L	5.9	1.0935085836560234	-10	14
Droplet in square	5.10	0.8979775098918368	-10	15

5.1. Setup of the Validation Test. Validation of the algorithm for the conformal mapping will be carried out in two cases, first we compare our algorithm with SC Toolbox in a convex and a non-convex quadrilateral. In the second test we parameterized the modulus of a rectangle and map it onto the unit disk.

The comparison to the SC Toolbox is carried out in the following quadrilaterals: convex quadrilateral $(\Omega; 0, 1, 1.5 + 1.5i, i)$ and non-convex quadrilateral $(\Omega; 0, 1, 0.3 + 0.3i, i)$, and line-segments joining the vertices as the boundary arcs. Then comparisons of the results obtained by the conjugate function method, presented in this paper, and SC Toolbox by Driscoll [8] are carried out. All SC Toolbox tests were carried with the settings `precision = 1e-14`. Comparison

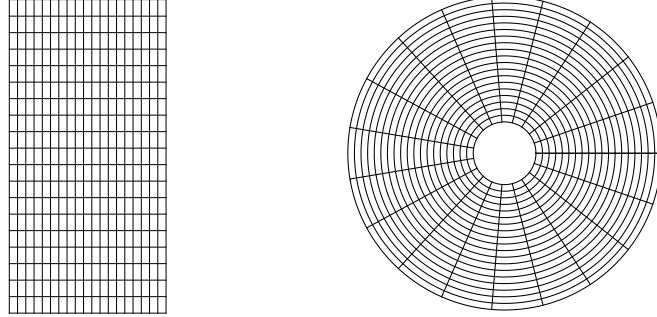


FIGURE 3. Canonical domains R_h and A_r on the left- and right-hand side, respectively.

is done by using the following test function

$$(3) \quad \text{test}(z) = |f(z) - g(z)|,$$

where f and g are obtained by the conjugate function method and SC Toolbox, respectively. The mesh setup of the quadrilaterals and the results are shown in Figure 4 and 5, respectively.

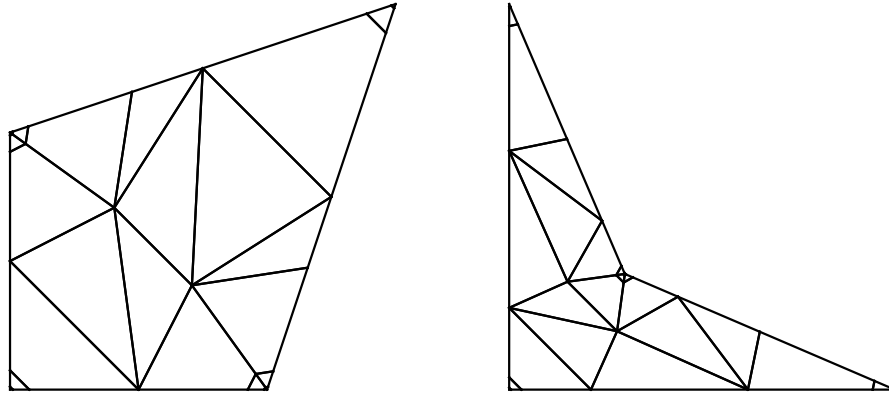


FIGURE 4. Geometric mesh of the convex (left-hand side) and the non-convex (right-hand side) quadrilateral used in computing the potential functions.

All our examples are carried out in the same fashion using the reciprocal identity (1) and a quadrilateral Q . The test function is

$$\text{rec}(Q) = |M(Q) M(\tilde{Q}) - 1|,$$

which vanishes identically. See also [11, Section 4].

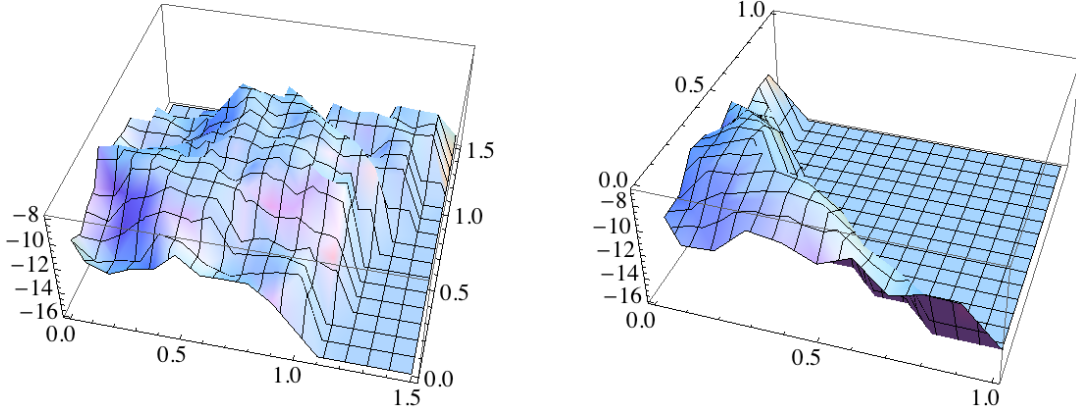


FIGURE 5. Comparison of the convex (left-hand side) and non-convex (right-hand side) quadrilateral between the conjugate function method and SC Toolbox. Result are obtained by taking the logarithm (with base 10) of the test function (3).

In the second validation test, we parameterized a rectangle respect to the modulus $M(Q)$ and map the rectangle onto the unit disk. The mapping is given by a composite mapping consisting a Jacobi's elliptic sine function and a Möbius transformation.

For every point (x_j, y_j) in the grid on the rectangle R_h , where $x_j = j/10$ and $y_j = jh/10$, $j = 0, 1, 2, \dots, 10$, we compute the error $\|e_j\|$ which is simply the Euclidean distance of the image of the initial point (x_j, y_j) computed by the conjugate function method and the analytical mapping. For a given modulus $M(Q)$ the values $\text{rec}(Q)$, $\max(\|e_j\|)$, and $\text{mean}(\|e_j\|)$, where the latter two represent the maximal and the mean error over the grid are presented in Table 4.

TABLE 4. The values of $\text{rec}(Q)$, $\max(\|e_j\|)$ and $\text{mean}(\|e_j\|)$ for a given $M(Q)$.

$M(Q)$	$\text{rec}(Q)$	$\max(\ e_j\)$	$\text{mean}(\ e_j\)$
1	$8.08242 \cdot 10^{-14}$	$1.87409 \cdot 10^{-8}$	$5.56947 \cdot 10^{-10}$
1.2	$6.35048 \cdot 10^{-14}$	$7.97889 \cdot 10^{-9}$	$7.49315 \cdot 10^{-10}$
1.4	$5.52891 \cdot 10^{-14}$	$1.21851 \cdot 10^{-8}$	$6.90329 \cdot 10^{-10}$
1.6	$8.85958 \cdot 10^{-14}$	$1.10001 \cdot 10^{-8}$	$7.90840 \cdot 10^{-10}$
1.8	$9.72555 \cdot 10^{-14}$	$1.19005 \cdot 10^{-8}$	$7.31645 \cdot 10^{-10}$
2	$9.41469 \cdot 10^{-14}$	$8.56068 \cdot 10^{-9}$	$7.67815 \cdot 10^{-10}$

5.2. Simply Connected Domains. In this section we consider a conformal mapping of a quadrilateral $Q = (\Omega; z_1, z_2, z_3, z_4)$ with curved boundaries $\gamma_1, \gamma_2, \gamma_3, \gamma_4$ onto a rectangle R_h such that the vertices z_1, z_2, z_3, z_4 maps to $1 + ih, ih, 0, 1$, respectively, and the boundary curves $\gamma_1, \gamma_2, \gamma_3, \gamma_4$ maps onto the line segments $\gamma'_1, \gamma'_2, \gamma'_3, \gamma'_4$. We give some examples and applications with illustrations. Simple examples of such domains are domains, where four or more points are connected with circular arcs. Some examples related to numerical methods and the Schwarz-Christoffel formula for such domains can be found in the literature, e.g., [5, 6, 15].

Example 5.1 (Unit disk). Let Ω be the unit disk. We consider a quadrilateral $Q = (\Omega; z_1, z_2, z_3, z_4)$, where $z_j = e^{i\theta_j}$, $\theta_j = (j - 1)\pi/2$. Note that, because of symmetry, it follows from (1) that the modulus is 1. The reciprocal error of the conformal mappings is $4.34 \cdot 10^{-14}$. This example was first given by Schwarz in 1869 [24].

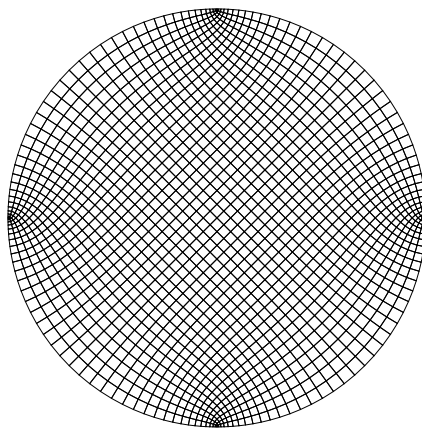


FIGURE 6. Example of the conformal map of a square onto a disk, first obtained by Schwarz in 1869 [24].

Example 5.2 (Flower). Let Ω be the domain bounded by the curve

$$(4) \quad r(\theta) = 0.8 + t \cos(n\theta),$$

where $0 \leq \theta \leq 2\pi$, $n = 6$ and $t = 0.1$. We consider a quadrilateral $Q = (\Omega; z_1, z_2, z_3, z_4)$, where $z_j = r(\theta_j)$, $\theta_j = (j - 1)\pi/2$, see Figure 7. As in Example 5.1, the modulus of Q is 1. The reciprocal error of the conformal mappings is $3.74 \cdot 10^{-11}$. Several other examples of flower shaped quadrilaterals are given in [11, Section 8.5].

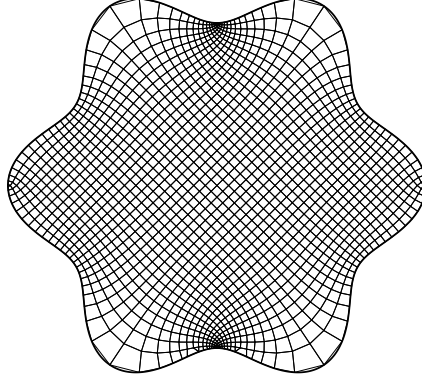


FIGURE 7. Illustration of the flower domain and the visualization of the pre-image of the rectangular grid (Figure 3).

Example 5.3 (Circular Quadrilateral). In [11] several experiments of circular quadrilaterals are given. Let us consider a quadrilateral whose sides are circular arcs of intersecting orthogonal circles, i.e., angles are $\pi/2$. Let $0 < a < b < c < 2\pi$ and choose the points $\{1, e^{ia}, e^{ib}, e^{ic}\}$ on the unit circle. Let Q_A stand for the domain which is obtained from the unit disk by cutting away regions bounded by the two orthogonal arcs with endpoints $\{1, e^{ia}\}$ and $\{e^{ib}, e^{ic}\}$, respectively. Then Q_A determines a quadrilateral $(Q_A; e^{ia}, e^{ib}, e^{ic}, 1)$. Then for the triple $(a, b, c) = (\pi/12, 17\pi/12, 3\pi/2)$, the modulus $M(Q_A) = 0.630587351084775$ and $M(\tilde{Q}_A) = 1.5858231191592544$. The reciprocal error of the conformal mapping is $1.68 \cdot 10^{-13}$.

Example 5.4 (Asteroïdal Cusp). Asteroïdal cusp is a domain Ω given by a

$$(5) \quad G_c = \{(x, y) : |x| < c, |y| < c\},$$

where $c = 1$ and the left-hand side vertical boundary line-segment is replaced by the following curve

$$r(t) = \cos^3 t + i \sin^3 t, \quad t \in [-\pi/2, \pi/2].$$

We consider a quadrilateral $Q = (\Omega; 1 - i, 1 + i, -1 + i, -1 - i)$. The reciprocal error of the conformal mappings is of the order 10^{-10} . The modulus $M(Q) = 0.68435408764536$ and $M(\tilde{Q}) = 1.4612318657235575$. Domain is illustrated in Figure 9.

5.3. Ring Domains. In this section we shall give several examples of conformal mapping from a ring domain R onto an annulus A_r . It is also possible to use the

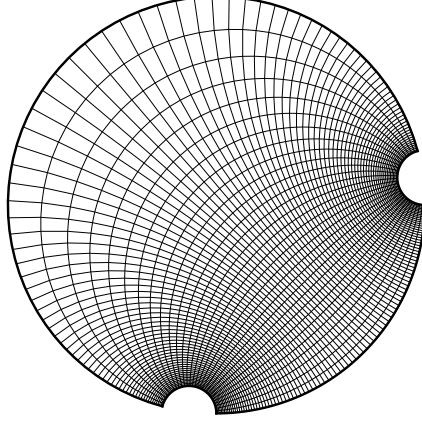


FIGURE 8. The quadrilateral $(Q_A; e^{i\pi/12}, e^{i17\pi/12}, e^{i3\pi/2}, 1)$ and the visualization of the pre-image of the rectangular grid (Figure 3).

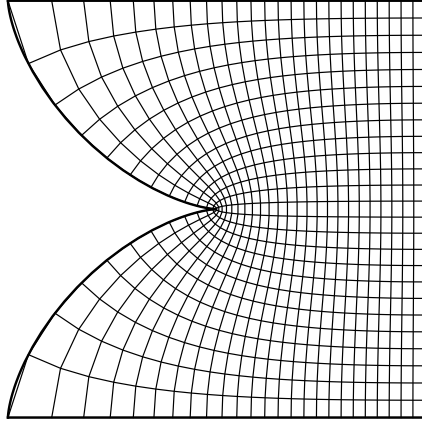


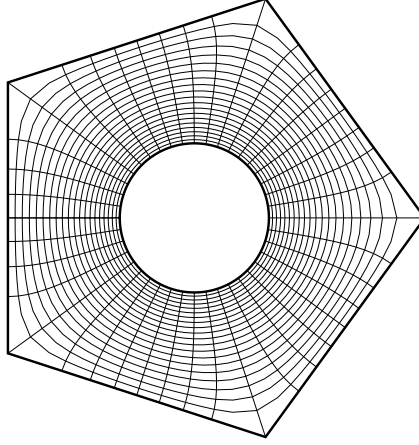
FIGURE 9. Asteroid cusp domain with the pre-image of the rectangular grid (Figure 3).

Schwarz-Christoffel method, see [13]. For symmetrical ring domains a conformal mapping can be obtained by using Schwarz' symmetries.

Example 5.5 (Disk in Regular Pentagon). Let Ω be a regular pentagon centered at the origin and having short radius (apothem) equal to 1 such that the corners of the pentagon are $z_k = e^{2\pi i k/5}$, $k = 0, 1, 2, 3, 4$. Let $\mathbb{D}(r) = \{z \in \mathbb{C} : |z| \leq r\}$. We consider a ring domain $R = \Omega \setminus \mathbb{D}(r)$ and compute the modulus $M(R)$ and the exponential of the modulus $e^{M(R)}$. Results are reported in Table 5 with the values $e^{M(R)}$ from [3, Example 5] in the fourth column.

TABLE 5. The values $M(R)$ and $e^{M(R)}$.

r	$M(R)$	$\exp(M(R))$	[3, Example 5]
0.1	2.35372035858745	10.524652459913115	10.5246525
0.4	0.9674246001764809	2.631159438480101	2.631159439
0.9	0.15070188000332954	1.1626499971978235	1.1626499972
0.99	0.03276861064365647	1.0333114143138304	1.03331141431
0.999	0.00934656029871744	1.0093903757950962	1.00939037579

FIGURE 10. Disk in pentagon ($r = 0.4$) with the pre-image of the annular grid (Figure 3).

Example 5.6 (Cross in Square). Let $G_{ab} = \{(x, y) : |x| \leq a, |y| \leq b\} \cup \{(x, y) : |x| \leq b, |y| \leq a\}$, and G_c as in (5), where $a < c$ and $b < c$. Then the domain cross in square is a ring domain $R = G_c \setminus G_{ab}$, see Figure 11. The reciprocal error of the conformal mapping is of the order 10^{-10} . The modulus $M(R) = 0.2862861647287473$.

Example 5.7 (Circle in Square). Let Ω be the unit disk. Then we consider a ring domain $R = G_c \setminus \Omega$, where $c = 1.5$, see Figure 12. The reciprocal error of the conformal mapping is of the order 10^{-14} . The modulus $M(R) = 0.9920378629010557$.

Example 5.8 (Flower in Square). Let Ω be a domain bounded by the curve (4). Then we consider a ring domain $R = G_c \setminus \Omega$, where G_c is given by (5) and $c = 1.5$. See Figure 13 for the illustration. The reciprocal error of the conformal mapping is of the order 10^{-9} . The modulus $M(R) = 0.6669554623348065$.

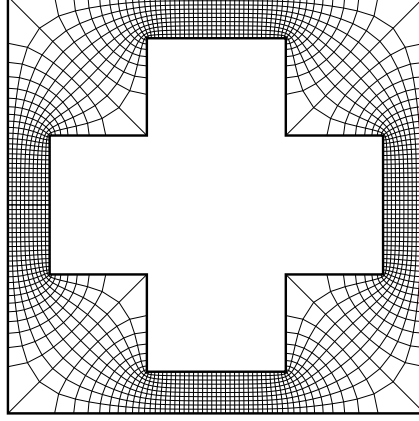


FIGURE 11. The ring domain $G_c \setminus G_{ab}$, where $a = 0.5, b = 1.2, c = 1.5$, with the pre-image of the annular grid (Figure 3).

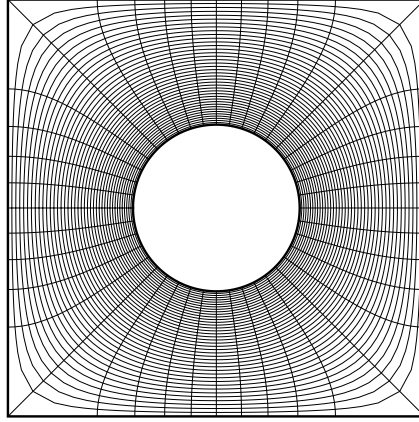


FIGURE 12. Disk in a square domain with the pre-image of the annular grid (Figure 3).

Example 5.9 (Circle in L). Let $L_1 = \{z \in \mathbb{C} : 0 < \operatorname{Re}(z) < a, 0 < \operatorname{Im}(z) < b\}$ and $L_2 = \{z \in \mathbb{C} : 0 < \operatorname{Re}(z) < d, 0 < \operatorname{Im}(z) < c\}$, where $0 < d < a, 0 < b < c$. Then $L(a, b, c, d) = L_1 \cup L_2$ is called an L-domain. Suppose that $\mathbb{D}(z_0, r) = \{z \in \mathbb{C} : |z - z_0| < r\}$. We consider a ring domain $R = L(a, b, c, d) \setminus \mathbb{D}(z_0, r)$, where $(a, b, c, d) = (3, 1, 2, 1)$, $z_0 = 8/5 + 2i/5$, and $r = 1/5$. See Figure 14.

In order to better illustrate the details of the mapping, a non-uniform grid has been used. For the real component the points x are

$$x = \{k/10 : k = 0, 1, \dots, 9\} \cup \{99/100, 999/10000, 9999/10000, 1\}.$$

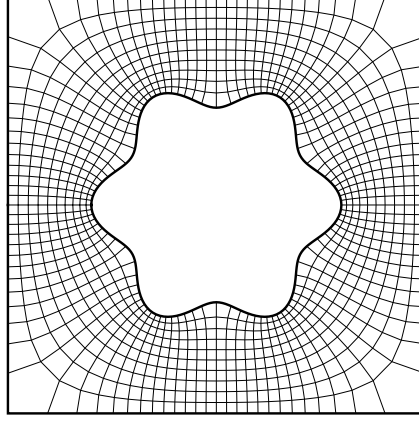


FIGURE 13. Flower in a square domain with the pre-image of the annular grid (Figure 3).

For the imaginary component the points y are chosen on purely aesthetic basis as:

$$y = \{k/10 : k = 1, 2, \dots, 9\} \cup \{0.316225, 0.324008, 0.327831, 0.329278, 0.331005, 0.687482\}.$$

The reciprocal error of the conformal mapping is of the order 10^{-10} . The modulus $M(R) = 1.0935085836560234$.

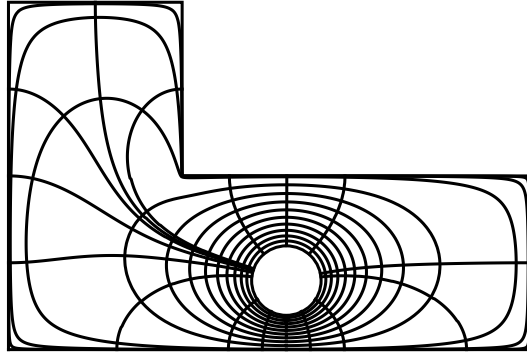


FIGURE 14. L-shaped domain with a circular hole with the pre-image of the non-uniform annular grid of Example 5.9.

Example 5.10 (Droplet in Square). Let Q_D be bounded by a Bezier curve:

$$r(t) = \frac{1}{640} (45t^6 + 75t^4 - 525t^2 + 469) + \frac{15}{32}t(t^2 - 1)^2i, \quad t \in [-1, 1].$$

Then the domain droplet in square is a ring domain $R = G_c \setminus Q_D$, where G_c is given in the first example concerning ring domains. For visualization, see Figure 15. The reciprocal error of the conformal mapping is of the order 10^{-10} . The modulus $M(R) = 0.8979775098918368$.

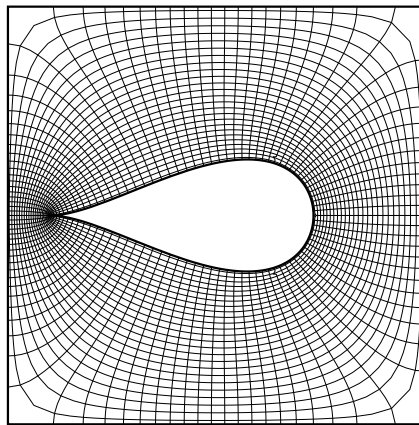


FIGURE 15. Droplet in square with the pre-image of the annular grid (Figure 3).

Acknowledgment. We thank R.M. Porter and M. Vuorinen for their valuable comments on this paper.

References

- [1] L.V. AHLFORS, *Conformal invariants: topics in geometric function theory*, McGraw-Hill Book Co., 1973.
- [2] L.V. AHLFORS, *Complex Analysis*, An introduction to the theory of analytic functions of one complex variable, Third edition. International Series in Pure and Applied Mathematics. McGraw-Hill Book Co., New York, 1978.
- [3] D. BETSAKOS, K. SAMUELSSON and M. VUORINEN, *The computation of capacity of planar condensers*, Publ. Inst. Math. 75 (89) (2004), 233-252.
- [4] J. BRANDTS, *The Cauchy-Riemann equations: discretization by finite elements, fast solution of the second variable, and a posteriori error estimation*, A posteriori error estimation and adaptive computational methods. Adv. Comput. Math. 15 (2001), no. 1-4, 6177 (2002).
- [5] P.R. BROWN, *Mapping onto circular arc polygons*, Complex Variables, Theory Appl. 50 (2005), No. 2, 131–154.

- [6] P.R. BROWN and R.M. PORTER, *Conformal Mapping of Circular Quadrilaterals and Weierstrass Elliptic Functions*, arXiv math.CV 1012.3495, 2010. Comput. Methods Funct. Theory (to appear).
- [7] D. CROWDY, *Exact solutions for the viscous sintering of multiply-connected fluid domains*. J. Engrg. Math. 42 (2002), no. 3-4, 225–242.
- [8] T.A. DRISCOLL, *Schwarz-Christoffel toolbox for MATLAB*, <http://www.math.udel.edu/~driscoll/SC/>
- [9] T.A. DRISCOLL and L.N. TREFETHEN, *Schwarz-Christoffel Mapping*. Cambridge Monographs on Applied and Computational Mathematics, 8. Cambridge University Press, 2002.
- [10] T.A. DRISCOLL and S.A. VAVASIS, *Numerical conformal mapping using cross-ratios and Delaunay triangulation*. SIAM J. Sci. Comput. 19 (1998), no. 6, 1783–1803.
- [11] H. HAKULA, A. RASILA, and M. VUORINEN, *On moduli of rings and quadrilaterals: algorithms and experiments*. SIAM J. Sci. Comput. 33 (2011), no. 1, 279–302.
- [12] P. HENRICI, *Applied and computational complex analysis. Vol. 3*. Discrete Fourier analysis—Cauchy integrals—construction of conformal maps—univalent functions. Pure and Applied Mathematics (New York). A Wiley-Interscience Publication. John Wiley & Sons, Inc., New York, 1986.
- [13] C. HU, *Algorithm 785: a software package for computing Schwarz-Christoffel conformal transformation for doubly connected polygonal regions*, ACM Transactions on Mathematical Software (TOMS), v.24 n.3, p.317-333, Sept. 1998
- [14] S.V. KRANTZ, *Geometric Function Theory*, Explorations in complex analysis. Cornerstones. Birkhuser Boston, Inc., Boston, MA, 2006.
- [15] V.V. KRAVCHENKO and R.M. PORTER, *Conformal mapping of right circular quadrilaterals*, Complex Variables and Elliptic Equations: An International Journal, 1–17, iFirst, 2010.
- [16] R. KÜHNAU, *The conformal module of quadrilaterals and of rings*, In: Handbook of Complex Analysis: Geometric Function Theory, (ed. by R. Kühnau) Vol. 2, North Holland/Elsevier, Amsterdam, 99-129, 2005.
- [17] P.K. KYTHE, *Computational conformal mapping*. Birkhuser Boston, Inc., Boston, MA, 1998.
- [18] O. LEHTO and K.I. VIRTANEN, *Quasiconformal mappings in the plane*, Springer, Berlin, 1973.
- [19] D.E. MARSHALL, *Zipper*, Fortran Programs for Numerical Computation of Conformal Maps, and C Programs for X-11 Graphics Display of the Maps. Sample pictures, Fortran, and C code available online at <http://www.math.washington.edu/~marshall/personal.html>.
- [20] D.E. MARSHALL and S. ROHDE, *Convergence of a variant of the zipper algorithm for conformal mapping*, SIAM J. Numer. Anal. 45 (2007), no. 6, 2577–2609 (electronic).
- [21] N. PAPAMICHAEL and N.S. STYLIANOPOULOS, *Numerical Conformal Mapping: Domain Decomposition and the Mapping of Quadrilaterals*, World Scientific Publishing Company, 2010.

- [22] R.M. PORTER, *History and Recent Developments in Techniques for Numerical Conformal Mapping*, Quasiconformal Mappings and their Applications (ed. by S. Ponnusamy, T. Sugawa and M. Vuorinen), Narosa Publishing House Pvt. Ltd., New Delhi, India (2007), 207-238.
- [23] R. SCHINZINGER and P.A.A. LAURA, *Conformal mapping: methods and applications*, Revised edition of the 1991 original. Dover Publications, Inc., Mineola, NY, 2003.
- [24] H.A. SCHWARZ, *Conforme Abbildung der Oberfläche eines Tetraeders auf die Oberfläche einer Kugel*, J. Reine Ange. Math., 70:121–136, 1869.
- [25] L.N. TREFETHEN, *Numerical computation of the Schwarz-Christoffel transformation*, SIAM J. Sci. Statist. Comput. 1 (1980), no. 1, 82–102.

Harri Hakula

E-MAIL: `harri.hakula@tkk.fi`

ADDRESS: *Aalto University, Institute of Mathematics, P.O. Box 11100, FI-00076 Aalto, Finland*

Tri Quach

E-MAIL: `tri.quach@tkk.fi`

ADDRESS: *Aalto University, Institute of Mathematics, P.O. Box 11100, FI-00076 Aalto, Finland*

Antti Rasila

E-MAIL: `antti.rasila@iki.fi`

ADDRESS: *Aalto University, Institute of Mathematics, P.O. Box 11100, FI-00076 Aalto, Finland*